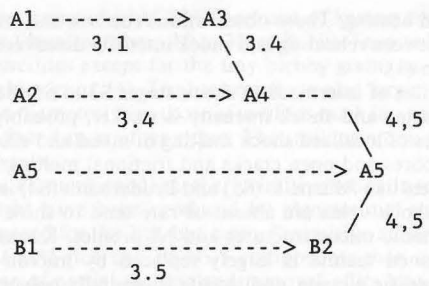

FIG. 1. Schematic of chondrule relationships and petrologic type of host.

(mesostasis and mineral grains). The resulting groups reflect both primary and secondary processes in a manner somewhat similar to the Van Schmus and Wood classes for chondrites (Table 1). The major difference is that chondrule metamorphism is not isochemical, and the group differences disappear at the highest metamorphic levels (Fig. 1). The Gooding-Keil system of nomenclature is still applicable, the McSween-Scott-Taylor types are integrated into the new system (*e.g.,* for Semarkona, types IA IB and II are included in A1, A2 and the B groups, respectively), and the 'droplet' and 'clastic' chondrules of Dodd are retained in that they roughly correspond to the A and B groups.

Compositional trends in the mesostasis, olivine and pyroxene, and the relative abundance of each chondrule group as a function of petrologic type, suggest that groups A1, A2, A5 and B1 are present in essentially unmetamorphosed material, and that during metamorphism these homogenize, via A3, A4 and B2, to equilibrated group A5, but at different rates. Thus in a given chondrite, the variety of chondrules present depends on (1) the variety originally present (which is remarkably constant from meteorite to meteorite), (2) the degree of metamorphism suffered by the host chondrite, (3) the responsiveness of the individual chondrules to metamorphism. Except for A5, the A series are fairly responsive to metamorphism, while the B series are more sluggish. Clearly, any study of chondrules has to take into account these complications, but sorting them into these 7 groups will help. To date we have only examined type 3 ordinary chondrites, but we suspect that the scheme will apply equally to chondrules in enstatite and carbonaceous chondrites.

Volatile loss during chondrule formation. D. W. G. Sears, Lu Jie and P. H. Benoit. Cosmochemistry Group, Dept. Chem. and Biochem., Univ. of Arkansas, Fayetteville, AR 72701, USA.

The question of Na-loss from chondrules has been controversial for over two decades. Many chondrules contain their cosmic complement of Na, which is surprising in view of the ease with which Na is lost in laboratory experiments (1). Either these chondrules were heated under very unusual conditions (2), or they were heated too briefly for Na loss. Many contain relict grains indicating the lack of complete melting (3). However, 35% of the chondrules in the essentially unmetamorphosed Semarkona chondrite not only show major depletions in Na, but also show volatility-related depletions in at least 6 moderately volatile elements (4, 5). They have distinctive cathodoluminescence (CL), which enables sorting into Group A1 (yellow CL mesostasis, with red CL ol/py, includes type IA, 4) and Group A2 (yellow CL mesostasis, little or no CL from the ol/py, includes PP). The better known 'Na-rich' chondrules, Group B (which include type II, 10), actually have flat CI-normalized abundance patterns, and none of their phases are cathodoluminescent (7).

Figure 1 shows liquidus temperatures, calculated by the method of ref. 8, 9, as a function of Na content for the chondrules from refs. 4, 7 and 10. A negative correlation between liquidus temperature and Na is clearly present among the Group A chondrules, which also implies a relationship between FeO and Na content since A2 generally have higher Fa than Al (7). The two chondrules furthest from the line have unusual characteristics, chondrule 28-12 is the only BO in Group A1 and chondrule 23-8 has atypically low CaO in its mesostasis. As expected, the Group B chondrules (10) show no evidence for a Na-liquidus temperature trend. In fact, since these chondrules probably did not reach the liquidus, their calculated temperatures are physically meaningless.

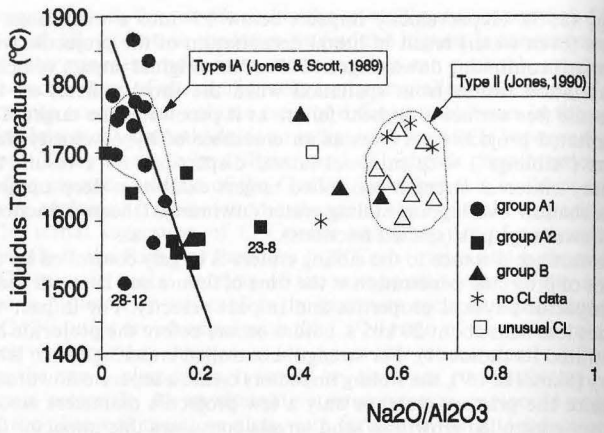

FIG. 1. Liquidus temperature *vs.* Na_2O/Al_2O_3 for chondrules from refs. 4, 5, 10.

We have argued that the reduction of silicates accompanied loss of volatiles during chondrule formation (5). Others have argued that the redox state and volatile content reflect precursor composition (*e.g.,* 4, 10). Hewins (9, quoting R. Jones) has suggested that if Na was lost during chondrule formation, then there would be negative correlation between liquidus temperature and Na, as we have observed for the Group A chondrules. The inverse zoning occasionally observed in the chondrule olivines, their small size relative to Group B chondrules and their elemental abundance patterns, which are volatility controlled, are additional evidence that, unlike Group B chondrules, Group A chondrules suffered reduction and devolatilization during chondrule formation. References: (1) Tsuchiyama *et al.* (1981) *GCA* **45,** 1357. (2) Wood (1988) *Protostars and Planets II,* 687. (3) Nagahara (1983) *Chondrules* 211. (4) Jones and Scott (1989) *PLPSC* **19th,** 523. (5) Lu *et al.* (1989) *LPS* **31,** 720. (6) DeHart (1990) Ph.D. thesis, Univ. Arkansas. (7) Lu *et al.,* this issue. (8) Herzberg (1979) *GCA* **43,** 1241. (9) Hewins (1991) *GCA* **55,** 935. (10) Jones (1990) *GCA* **54,** 1785.

An experimental study of Mg self-diffusion in spinel. Y. J. Sheng, I. D. Hutcheon and G. J. Wasserburg. The Lunatic Asylum, Div. of Geological and Planetary Sciences, Caltech, Pasadena, CA 91125, USA.

Mg isotope heterogeneity, both between coexisting spinel and silicates and among spinels, is a prominent feature of Plagioclase-Olivine Inclusions (POIs) (1). The preservation of isotopic heterogeneity and relict spinel (Sp) in inclusions with igneous textures indicates that the thermal event which partially melted the precursor material either had too low a temperature or was too brief to allow Mg isotope homogenization between Sp and the melt. Since the temperature history required to homogenize Mg isotopes depends on the diffusion rate of Mg in Sp, we designed experiments using an isotope tracer method to determine this critical rate (2). The diffusion couple consists of a gem quality $MgAl_2O_4$ Sp wafer and ^{25}Mg-doped glass of POI composition. The bulk compositions of starting glasses were chosen from phase equilibria data (3) to be Sp-saturated at the run temperature of a given experiment. The presence of chemical equilibrium between glass and Sp for each run ensures that Mg diffuses only in response to the isotopic disequilibrium. Glasses were verified to be chemically and isotopically homogeneous and were then equilibrated at a temperature slightly below the spinel saturation temperature of the melt to ensure chemical equilibrium. Polished Sp wafers were pre-annealed for 24 hr at 1500 °C. The polished surfaces of the Sp wafer and glass were placed together and held at temperatures between 1260 and 1550 °C for 20 to 0.5 hr. Mg isotope profiles in Sp and glass were measured with the PANURGE ion microprobe (4, 5) across a traverse perpendicular to the diffusion interface. Measured $^{25}Mg/^{24}Mg$ ratios were corrected for differences in isotopic fractionation between Sp and glass by normalizing to $^{26}Mg/^{24}Mg = 0.13955$. The diffusion coefficients (D) were calculated from the measured isotope profiles using a model that includes the complimentary diffusion of ^{24}Mg, ^{25}Mg and ^{26}Mg in both phases with the constraint that

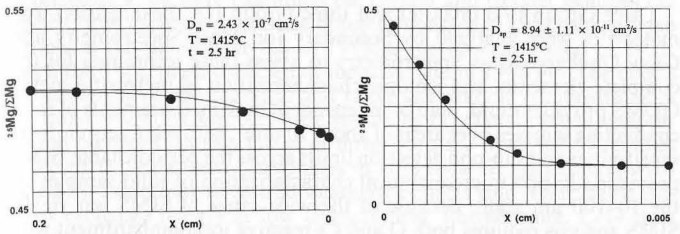

FIGS. 1, 2. Variation of $^{25}Mg/\Sigma Mg$ across a traverse in glass (Fig. 1) and Sp (Fig. 2) for the experimental run at 1415°C. The fitted curve is the calculated diffusion profile.

the Mg content of each phase is constant. Diffusion profiles measured in Sp and glass for the experimental run at 1415 °C are shown in Fig. 1, 2. The temperature dependence of D for Mg self diffusion in Sp is obtained from an Arrhenius relation. The activation energy and pre-exponential factor are, respectively, 395 ± 8 kJ and 162.6 ± 1.1 cm^2/s. For a maximum melting temperature for POIs of ~1500 °C (3) these results show that a 10 μm radius Sp would equilibrate isotopically with a melt within 60 min. To preserve isotopic heterogeneity, the POIs must have initially cooled faster than 50 to 250 °C/hr. References: (1) Sheng Y. *et al.* (1991) *GCA* **55,** 581. (2) Sheng Y. *et al.* (1991) *LPSC* **22,** 1233. (3) Sheng Y. *et al.* (1991) *LPSC* **22,** 1231. (4) Huneke J. *et al.* (1983) *GCA* **47,** 1635. (5) Hutcheon I. *et al.* (1987) *GCA* **51,** 3175.

Profiles of Ti^{3+}/Ti^{tot} ratios in zoned fassaite in Allende refractory inclusions. S. B. Simon[1] and L. Grossman.[1,2] [1]Dept. of Geophysical Sciences, [2]Enrico Fermi Institute, The University of Chicago, Chicago, IL 60637, USA.

In the fassaite found in Allende Type B, Ca-, Al-rich inclusions (CAI's), Ti is compatible and decreases in abundance from crystal cores to rims. This trend reflects crystallization-induced depletion of Ti in the residual liquid. $D_{Ti^{3+}}^{fas/L}$, the fassaite crystal/liquid distribution coefficient for Ti^{3+}, is greater than $D_{Ti^{4+}}^{fas/L}$, and Allende fassaite generally has $Ti^{3+}/Ti^{tot} > 0.5$, where $Ti^{tot} = Ti^{3+} + Ti^{4+}$ per six oxygen ions. Crystallization of fassaite from a CAI melt might therefore be expected to have depleted the residual liquid in Ti^{3+} relative to Ti^{4+}, *if* the residual liquid did not re-equilibrate with a reducing gas to restore the original Ti^{3+}/Ti^{tot} ratio. To investigate whether buffering occurred, we conducted electron probe traverses across two subliquidus fassaite crystals in each of TS22 (Type B2) and TS23 (B1), three in TS33 (B1) and four in TS34 (B1). Because of the large uncertainty in Ti^{3+}/Ti^{tot} at low TiO_2^{tot} contents, we restrict our discussion to the parts of the traverses with TiO_2^{tot} >4 wt.%, but all are between 500 and 1000 μm long. Four traverses, two each in TS22 and TS33, are flat except for sharp drops at the points nearest the rims where TiO_2^{tot} >4 wt.%. For example, in TS33 crystal 1 the Ti^{3+}/Ti^{tot} ratio drops from 0.709 ± .030 to 0.516 ± .058, and in TS33 crystal 2, from 0.707 ± .013 to 0.467 ± .030. The four TS34 traverses show progressive core-rim decreases in Ti^{3+}/Ti^{tot} but, in addition, near their rims, three of the four have sharp increases in Ti^{3+}/Ti^{tot} (*e.g.,* from 0.512 ± .032 to 0.776 ± .023), TiO_2^{tot} (4.7 to 6.7 wt.%) and V_2O_3 (0.07 to 0.29 wt.%) followed by sharp decreases in Ti^{3+}/Ti^{tot}. Ion probe analyses of one of the TS34 crystals show progressive core-rim increases in trivalent REE concentrations, and a decrease in Sr and a leveling off of Eu contents just before the Ti spike.

Fractional crystallization models (with $D_{Ti^{3+}}^{fas/L} \sim 3$ and $D_{Ti^{4+}}^{fas/L} \sim 1$) predict slight, gradual decreases in Ti^{3+}/Ti^{tot} during most of the interval of fassaite crystallization, with sharp drops toward the end of crystallization. The trends in TS22, TS33 and TS34 are in very good agreement with these models, indicating that the Ti^{3+}/Ti^{tot} ratios in fassaite are consistent with control by fractional crystallization without re-equilibration of the residual liquid with the surrounding, solar nebular, reducing gas. This is not surprising, especially in the case of TS34. This inclusion has reversely zoned melilite, indicating a minimum cooling rate of 0.5 °C/hr and a maximum of ~50 °C/hr (1). Fassaite crystallizes over a temperature range of ~50 °C (2), giving the liquid a maximum of ~100 hr, but possibly as little as 1 hr, in which to re-equilibrate with the gas. Also, in Type B inclusions, fassaite crystallizes late, and isolation of liquid from the gas might be expected, especially toward the end of fassaite crystallization when the inclusions would have been almost completely solidified. The sharp drops in Ti^{3+}/Ti^{tot} correspond to this part of the crystallization history. One inclusion, however, has flat patterns: TS23, at 0.545 ± .068 and 0.627 ± .069, suggesting that gas-liquid equilibrium was maintained throughout the interval of fassaite crystallization. This is not easily explained, because this inclusion is a Type B1 with reversely zoned melilite. The melilite mantle should have isolated the residual melt, and re-equilibration was subject to the same time constraint as described above. Perhaps parts of the mantle remained liquid long enough to allow communication with the reducing gas until after the TiO_2^{tot} of fassaite dropped below 4 wt.%.

The Ti spikes in late fassaite in TS34 reflect the onset of anorthite crystallization. From the reversely zoned melilite in this inclusion, we know that fassaite began crystallizing before anorthite (1). Anorthite was supersaturated (activity > 1) during fassaite crystallization and, just before anorthite precipitated, its activity may have increased sharply, causing an increase in the Ti^{3+}/Ti^{tot} ratio due to the reaction $4T_4P + Di + 3An \rightleftharpoons 4T_3P + 4CaTs + Sp + O_2$ (3). When anorthite crystallized, its activity fell to 1, causing a decrease in the Ti^{3+}/Ti^{tot} in the co-crystallizing fassaite. Anorthite precipitation depleted the residual melt in Sr and Eu and increased its Ti and V contents, and these changes were recorded in the co-crystallizing fassaite. Ti enrichment was delayed relative to Sr depletion in the fassaite because, unlike Sr, Ti is a stoichiometrically constrained major element which enters pyroxene as $CaTi^{3+}AlSiO_6(T_3P)$ and $CaTi^{4+}Al_2O_6(T_4P)$, making its concentration in fassaite dependent not only on its own concentration in the melt but also on the concentrations of other major elements. Acknowledgements: We thank J. R. Beckett for helpful discussions and A. M. Davis for ion probe analyses. This work was supported by NASA grant NAG 9-54. References: (1) MacPherson G. J. *et al.* (1984) *J. Geol.* **92,** 289–305. (2) Beckett J. R. (1991) pers. comm. (3) Beckett J. R. (1986) Ph.D. thesis, University of Chicago.

Cross sections for production of carbon-14 from oxygen and silicon: Implications for cosmogenic production rates. J. M Sisterson,[1] A. J. T. Jull,[2] D. J. Donahue,[2] A. M. Koehler,[1] R. C. Reedy[3] and P. A. J. Englert.[4] [1]Harvard Cyclotron Laboratory, Harvard University, Cambridge, MA 02138, USA. [2]NSF Accelerator Facility for Radioisotope Analysis, University of Arizona, Tucson, AZ 85721, USA. [3]Space Science and Technology Division, Los Alamos National Laboratory, Los Alamos, NM 87545, USA. [4]Dept. of Chemistry, San Jose State University, San Jose, CA 92521, USA.

The study of radioisotopes of differing half-lives in lunar rocks and cores gives valuable information about the constancy of the solar cosmic-ray (SCR) and galactic cosmic-ray fluxes and about the samples' recent histories. Determinations of SCR fluxes in the past depend on the accuracy of the cross sections. The cross sections for production of many radioisotopes from particles of SCR energies are often not well known (1). One such set of cross sections is that for $^{16}O(p,3p)^{14}C$; these data are important for interpretation of the 14C depth-profile data from Apollo 15 cores (2), lunar rocks (3) and some meteorites. Some re-evaluated or previously unpublished cross section measurements for the reaction $^{16}O(p,3p)^{14}C$ in proton energy range 25–160 MeV were recently reported (4).

In this paper, we report on some new measurements for the cross sections for ^{14}C production from oxygen and silicon in the proton energy range of 58.5 to 158 MeV. Nine sets of SiO_2 (quartz) and silicon targets were irradiated at the Harvard Cyclotron Laboratory and the number of protons through each target ranged from about 0.7 to about 1.3 × 10^{14}. The samples were analyzed at Arizona, where the samples were crushed and melted in an RF furnace with iron in a flow of oxygen (5). The resulting gas was oxidized to CO_2, and diluted to about 1 cm^3 volume. The diluted gas is reduced to graphite (5) and pressed into an accelerator target. Analysis for 14C was performed by accelerator mass spectrometry (6). The data from the quartz samples have been analyzed and give preliminary values of about 2.1 to 2.8 mb for the $^{16}O(p,3p)^{14}C$ cross section in the energy range 58-158 MeV. After the analysis of the silicon targets is completed, these values will be corrected for the contribution to the cross section from $natSi(p,x)^{14}C$. Measurements at lower proton energies, down to threshold, are planned using the Davis cyclotron. The results appear to confirm the magnitude of previous estimates (7, 8) of the production cross sections for ^{14}C from oxygen with reduced